.

# A GMSK/PAM4 Multi-Channel Magnetic Human Body Communication Transceiver

Miao Meng, Member, IEEE, Hossein Rahmanian Kooshkaki, Student Member, IEEE, Xiaoyang Wang, Student Member, IEEE, Shih-Kai Kuo, Student Member, IEEE, Erda Wen, Student Member, IEEE and Patrick P. Mercier, Senior Member, IEEE

Abstract—This letter presents a dual-mode multi-channel transceiver implemented with low path loss offered by magnetic human body communication (mHBC) towards ultra-efficient body-area networking. Two spectral efficient modulation schemes, GMSK and PAM4, are used to reduce interference on adjacent channels. A power oscillator is used to efficiently generate both GMSK and PAM4 modulated magnetic fields while multi-channel selection is implemented by on-chip capacitor tuning and an analog PLL, enabling 5Mbps and 10Mbps data for GMSK and PAM4, respectively. The transmitter achieves an efficiency of 15.5 and 19.4 pJ/bit, while the receiver consumes 4.6 and 2.7 pJ/bit for GMSK and PAM4, respectively.

Index Terms—magnetic human body communication, WBAN, energy/spectral efficiency, low-power receiver, GMSK, PAM4.

## I. INTRODUCTION

Wireless internet connectivity is essential for most wearable devices such as wireless headphones, smart glasses, and medical monitoring sensors. Instead of individually accessing the internet, a local body area network (BAN) offers a way to efficiently connect wearables to a central unit (smartphone or smartwatch), which then communicates using commodity wireless equipment. Reducing the communication distance to cover only the body ideally reduces the power consumption within the wearable device, enabling a smaller form factor implementation that can comfortably fit within the confines of human anatomy [1]. However, since biological tissue absorbs energy very well at conventionally used radio frequencies (e.g., 2.4GHz), the path loss incurred by conventional RF approaches can be quite large [2], reducing the impact of power reduction in a BAN.

Instead of broadcasting RF power, electric-field-based human body communication (eHBC) schemes have been demonstrated, showing improved energy efficiency due to lower path loss around the human body compared to conventional methods [3]–[5]. However, the actual path loss experienced by eHBC is often higher than what is reported due to difficulties in making accurate measurements [6]. Moreover, capacitive coupling to the body in eHBC is susceptible to changes in posture and normal movements, making robust operation over a wide range of conditions difficult, given the typical need for variable inductive tuning.

An alternative BAN approach is to use magnetic fields, offering equivalent or in some cases superior path loss to eHBC

M. Meng and X. Wang were and H. R. Kooshkaki, S. Kuo, E. Wen and P. Mercier are with the Department of Electrical and Computer Engineering, University of California at San Diego, La Jolla, CA 92093 USA. (e-mail: pmercier@ucsd.edu). M . Meng is now with College of Electronic and Information Engineering, Tongji University, Shanghai, China.(e-mail: miaomeng@tongji.edu.cn)

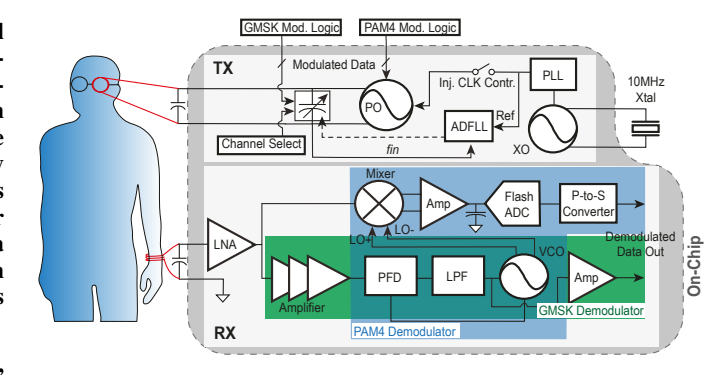


Fig. 1. Block diagram of the proposed mHBC transceiver.

approaches, yet with lower environmental/posture variation and easier variable capacitive tuning (mHBC) [7]. Previous work has demonstrated an on-off-keying (OOK) modulated mHBC transceiver with sub-10pJ/bit energy efficiency and 5Mbps data rate [1]. However, this previous mHBC transceiver implemented simple OOK modulation with low-complexity transmitter (TX) and receiver (RX) structures that limit the data rate and spectral efficiency. In addition, multi-channel communication was not supported, which is important towards supporting multiple device on-body at once.

This paper presents a dual-mode, multi-channel mHBC transceiver with improved data rate and spectral efficiency to enable potentially simultaneous multi-channel operation and add a degree of freedom to select the most efficient modulation scheme based on the application. Two modulation schemes, namely Gaussian-Minimum-Shift-Keying (GMSK) and 4-level Pulse-Amplitude Modulation (PAM4), are implemented while supporting multi-channel access. In addition, TX power level adjustability is also added to allow power level tunability according to the application needs.

## II. SYSTEM AND CIRCUIT IMPLEMENTATION

Fig. 1 shows the block diagram of the proposed dual-mode multi-channel mHBC transceiver (TRX). The TX uses a direct-RF power oscillator (PO), where the mHBC coil is directly used as a resonant element. GMSK modulation is performed by switching a capacitive DAC (CDAC) connected to the coil, while PAM4 modulation is achieved by adjusting the oscillation amplitude through tail current control. To have a fast start-up (less than Q cycles), and also ensure the PO frequency is robust against inductance variations of the wearable coil, an injection locking mechanism along with an ADFLL (the same as [1]) are employed. However, the injection locking signal in this work (used only in PAM4 mode) is provided by an analog PLL (rather than only the

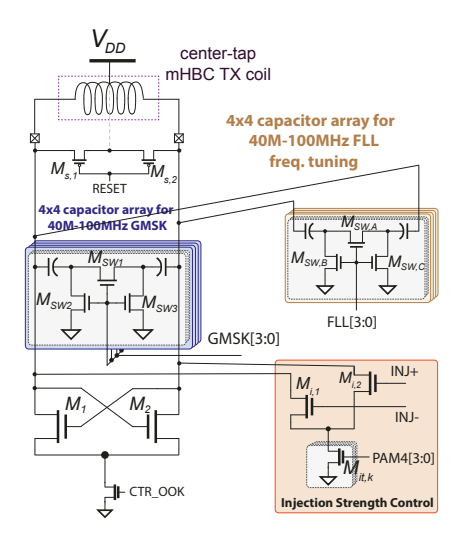


Fig. 2. Schematic of proposed power oscillator TX for fast-data-rate communication and with dynamic resonant frequency calibration.

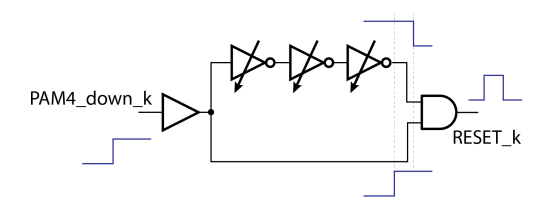


Fig. 3. Schematic of reset pulse width generator.

crystal oscillator), enabling multi-channel TX operation by changing the output frequency of the analog PLL. In GMSK mode, the RX uses another analog PLL whose control voltage is used for demodulating GMSK data. In PAM4 mode, the PLL output drives a passive mixer in a zero-IF architecture to demodulate PAM4 data.

## A. TX Power Oscillator

The 40-100 MHz TX is shown in Fig. 2. The direct-RF PO provides inherent impedance matching to the employed coil, and can be readily gated down to very low leakage power levels. Compared to a conventional PO, an additional capacitor array and injection transistors are used in the PO to support both GMSK and PAM4. The main capacitor array  $(M_{sw,1}, M_{sw,2}, M_{sw,3})$  is used for channel selection.

In GMSK mode, first, a channel selection code is applied to the main 4x4 capacitor array (4 channels, each with 4-bit tunable capacitor array) to ensure that only the capacitors of the selected channel are enabled, and others are disconnected from the LC tank, as shown in Fig. 2. Then, the connection of the 4-bit binary capacitors is controlled by code GMSK[3:0] to perform GMSK.

Since the Q of the TX coil can be large (e.g., 50), the PO usually has a long start-up and turn-off time when the oscillation amplitude is only controlled by the tail transistor in the main branch ( $CTR\_OOK$ ). This would nominally limit the available data rate in the PAM4 mode. To address this, transistors  $M_{i,1,2}$  and  $M_{s,1,2}$  are used to accelerate the amplitude transitions and enable a 10Mbps data rate. Transistors  $M_{i,1,2}$  are used as a pair of shunt injection transistors to inject

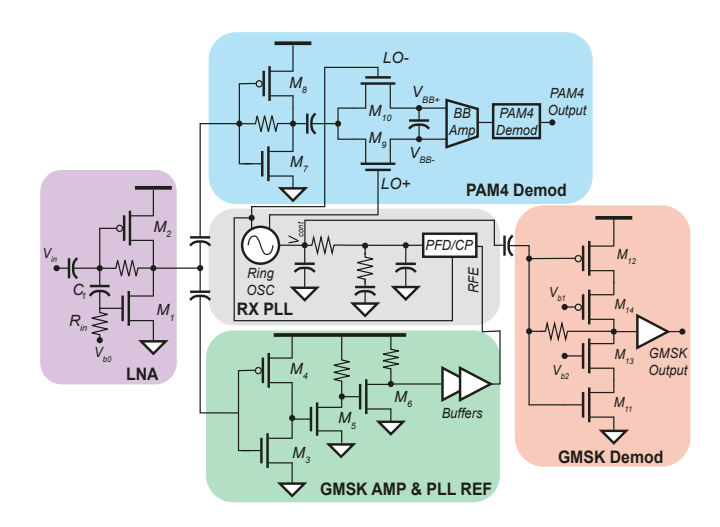


Fig. 4. Circuit details of the proposed dual-mode RX.

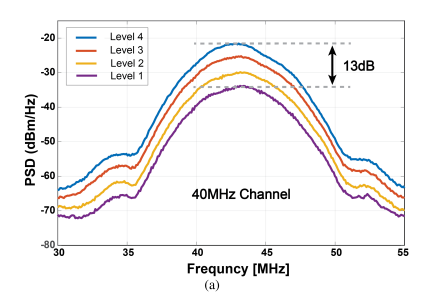
more current into the LC tank to help the oscillation amplitude rapidly ramp up and set the steady-state oscillation amplitude, while transistors  $M_{s,1,2}$  are implemented to help the amplitude rapidly go down between different PAM4 levels. The 4-level oscillation amplitude and amount of current injected into the LC tank are controlled by the 4-bit tail-current transistors  $M_{it,k}$  in the injection branch.

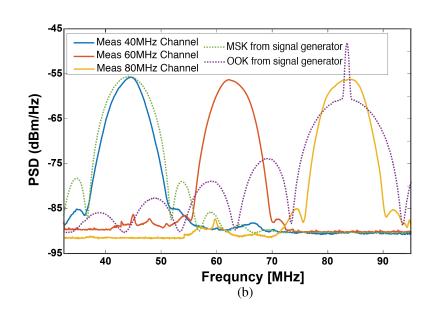
Since the resonant frequency of the PO can vary slightly with posture or environmental variations in the  $\sim$ ms timescale, an analog PLL is used to set the rate at which the injection currents are applied, while an ADFLL dynamically tunes the oscillation frequency using a 4x4 fine-tuning capacitor array  $(M_{sw,A}, M_{sw,B}, \text{ and } M_{sw,c})$  controlled by code FLL[3:0] as shown in Fig. 2 [1], all between packet transmissions. Because the shunt strength requirements of different transitions are different in the PAM4 mode (e.g., the required shunt strength of level 4 to level 1 transition is much larger than level 4 to level 3 transition), a variable reset pulse width generator is used, as shown in Fig. 3. When a falling transition of the PAM4 amplitude is detected, a rising edge is sent to the pulse width generator whose output pulse width is based on the initial and the final level of the PAM4 signal. This pulse is then buffered and sent to turn on the shunt transistors to help a rapid falling transition.

### B. Receiver Circuit Implementation

Fig. 4 shows circuit details of the proposed dual-mode receiver. The real part of the input impedance  $(R_{in})$  is designed to be matched to the loss of the input coil  $(3k\Omega)$  for maximum power transfer at the frequency of interest. Both GMSK and PAM4 modes share a self-biased LNA structure  $(M_1, M_2)$  that amplifies the input signal by more than 23dB. Gain adjusting mechanisms are adopted by the LNA structure  $(M_1, M_2)$  and the mixer driver  $(M_7, M_8)$ , providing 16dB gain adjustability to prevent the signals from saturation without changing the input matching. The  $V_{DS}$  voltage of  $M_1$  at DC is decoupled from its  $V_{GS}$  by  $C_1$ , enabling the LNA to work properly with a low  $V_{DD}$  of 0.6V.

The PAM4 mode is designed to utilize a zero-IF structure, using a passive mixer  $(M_9, M_{10})$  and a mixer driver  $(M_7, M_8)$ .





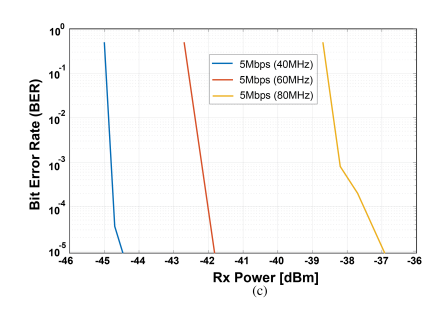
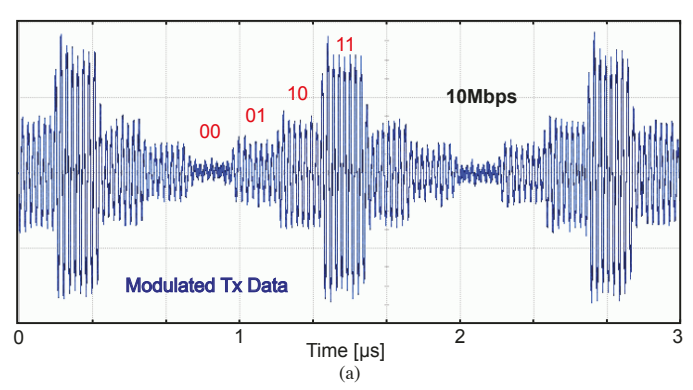


Fig. 5. GMSK transceiver measurement results. (a) Different TX power levels for 40MHz channel, (b) Non-overlapping adjacent channels compared with ideal MSK and OOK spectrum, (c) BER for different channels.



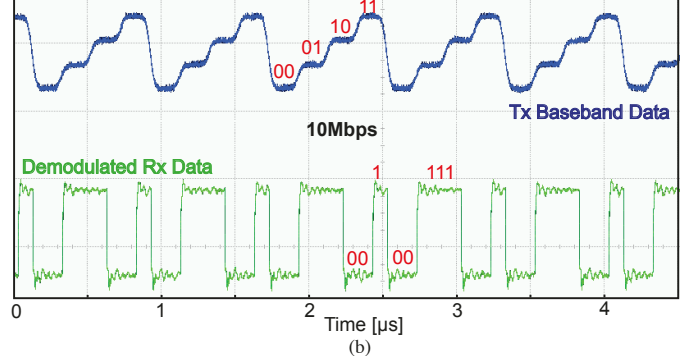


Fig. 6. Measured PAM4 transient waveform. (a) Modulated TX data. (b) TX baseband data and demodulated data.

The driver ensures that the input impedance of the mixer does not degrade the LNA gain. The LO signals driving the passive mixer are generated by an analog PLL whose reference is provided by the amplified (rail-to-rail) version of the input signal with proper phase alignments. To achieve such a rail-to-rail signal, an additional low-power 3-stage amplifier ( $M_3$ - $M_6$ ) based on [8] is utilized. The PAM4 baseband signal ( $V_{BB+}, V_{BB-}$ ) is amplified up to 24dB by an additional baseband amplifier (BB Amp) with tunable gain and bandwidth followed by a 2-bit flash ADC and a parallel-to-serial converter with shared RX clock as the PAM4 demodulator.

The analog PLL is reused for GMSK demodulation, since the PLL reference signal is also the rail-to-rail version of the input GMSK signal. The control voltage of PLL  $(V_{cont})$  contains the demodulated GMSK signal, which is amplified by 36dB using a cascode amplifier structure  $(M_{11}\text{-}M_{14})$  before going to the output buffer.

### III. MEASUREMENT RESULTS AND CONCLUSION

The chip was fabricated in a 65nm CMOS process, using a 0.7V supply for TX and a 0.6V supply for RX. During testbench measurements, the wire-wound TX and RX coils were separated by 10 cm distance in the air (pre-measured 12-dB-path-loss) with quality factors of  $\sim 50$  and  $\sim 10$ , respectively. The TX consumes 65.5 $\mu$ W and 182 $\mu$ W under GMSK and PAM4 modes, when the output power levels are -23dBm and -11dBm, respectively. The RX consumes  $23\mu$ W and  $27\mu$ W for GMSK and PAM4, respectively. When a  $12\mu$ W crystal oscillator for the reference clock is included, TX and

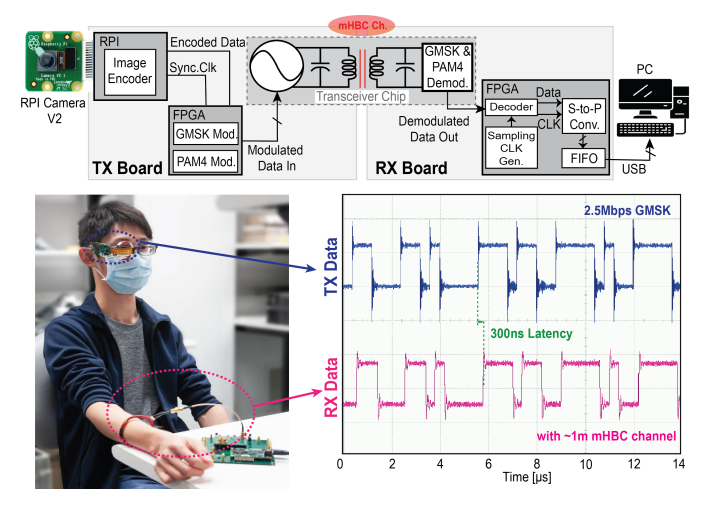


Fig. 7. A smart-glass video streaming demonstration.

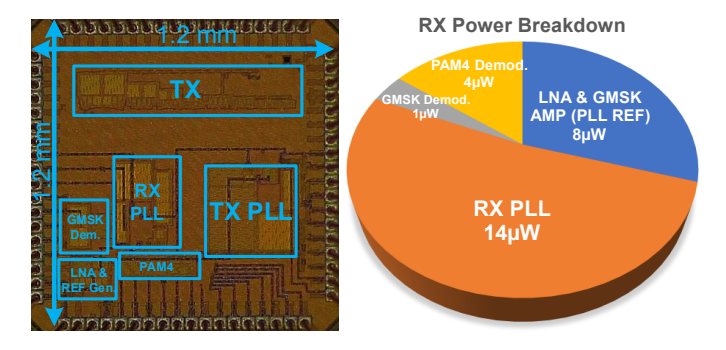


Fig. 8. The die micrograph and RX power breakdown.

	Cho JSSC'16 [3]	Saadeh JSSC'17 [4]	Maity JSSC'19 [5]	Park JSSC'19 [1]	This work	
HBC scheme	eHBC	eHBC	eHBC	mHBC	mHBC	
Multi-channel	No	Yes	No	No	Yes	
Freq. band [MHz]	20-60/140-180	20-120	0-15	37.5-42.5	40-100	
Modulation	BPSK	P-OFDM BPSK	Direct Digital	OOK	GMSK	PAM4
Maximum data rate [Mbps]	80	2	30	5	5	10
TX output power [dBm]	NA	NA	NA	-24.8	-23	-11
TX power consumption	1.7-2.6mW	0.87mW	93μW	35.8μW	65.5μW	182μW
TX E/bit [pJ/bit]	79(TRX link)	435	3.1	7.15*	15.5*	19.4*
RX sensitivity [dBm]	-58	-83.1	-63.3	-56	-45△	-35†∆
RX power consumption	6.3mW	1.1mW	98μW	23.5μW	23μW	27μW
RX E/bit [pJ/bit]	79(TRX link)	550	3.27	4.7*	4.6*	2.7*
CMOS process	65nm	65nm	65nm	65nm	65nm	

<sup>\*</sup>Including the power of frequency generation/synthesis.

†Measured with fixed data pattern.

4Gain limited sensitivity instead of noise limited.

RX efficiencies of 15.5pJ/bit and 4.6pJ/bit are achieved for GMSK, while 19.4pJ/bit and 2.7pJ/bit are achieved for PAM4. Fig.5a shows 13dB of TX tunability for GMSK at 40MHz, which can help enable more efficient operation when link budgets permit. Fig.5b depicts the superimposed TX spectra of three channels with 5Mbps data rate in the GMSK mode, where each channel occupies 5MHz with an additional 5MHz of spacing. Ultimately, up to 6 distinct channels could be supported from 40-100MHz. As compared to measured OOK and MSK signals from a signal generator, the implemented GMSK spectra has significantly less sidelobes and spillover into adjacent channels, thereby reducing interference and enabling tighter channel spacing.

The measured bit error rate (BER) of three channels for 5Mbps GMSK is shown in Fig. 5c, with pseudo-random data, achieving sensitivities of -44.8dBm, -42.2dBm, and -38.4dBm for 40MHz, 60MHz, and 80MHz channels with BER of  $10^{-3}$ . It should be noted that the BER for the proposed system is limited by the gain (and not the noise) of the LNA and the PLL REF circuits, since the received signal is used as a reference for the PLL and must therefore be very large. However, the achieved sensitivity is more than enough for the proposed system thanks to the low path loss provided by mHBC [7]. Fig.6 shows the measured PAM4 transient waveform. The 10Mbps-PAM4-modulated TX data with 40 MHz carrier is shown in Fig.6a. Fig.6b shows the correctly demodulated data in LSB-first order as compared to the TX baseband data.

To demonstrate that the designed mHBC TRX is capable of operating in a practical wearable application, a smart-glasses-to-smart-watch video data streaming system is developed. As shown in Fig. 7, the TX coil is wound on a pair of glasses, while the RX coil is worn on the wrist. A Raspberry Pi camera with a Sony Exmor IMX219 sensor is connected to a Raspberry Pi Zero - the most compact size in the Raspberry Pi family. Video frames are transmitted from Raspberry Pi to the FPGA via SPI and encoded in the FPGA to be transmitted via the mHBC channel. The mHBC TX generates a 40 MHz 2.5-Mbps GMSK-modulated signal with the TX coil. The demodulated data stream from mHBC is sampled by the FPGA internal clock, parallelized by a serial-to-parallel converter, buffered in a FIFO, and sent to a PC via USB. Fig.7 shows the demonstration block diagram, setup, transient waveforms,

and the corrected demodulated data with only 300ns latency. Simultaneous operation of multiple transceiver pairs operating on different frequencies will be investigated in future work. Fig.8 shows the die micrograph and the RX power breakdown. The chip has an active area of  $0.8mm^2$ .

Table I shows the performance summary and comparison with the prior work. The proposed design supports multi-channel human body communication with two more spectrally-efficient modulation schemes than prior mHBC work. The proposed mHBC PAM4 RX achieved the lowest energy consumed per bit, even though the energy cost of the frequency synthesis is included. The proposed GMSK RX has approximately the same energy efficiency as the OOK scheme used in [1], though here with superior spectral efficiency and significantly less inter-channel interference.

#### REFERENCES

- J. Park and P. P. Mercier, "A Sub-10-pJ/bit 5-Mb/s Magnetic Human Body Communication Transceiver," in *IEEE Journal of Solid-State Circuits*, vol. 54, no. 11, pp. 3031-3042, Nov. 2019.
- [2] J. Edelmann and T. Ussmueller, "Can You Hear Me Now?: Challenges and Benefits for Connectivity of Hearing Aids and Implants," in *IEEE Microwave Magazine*, vol. 19, no. 7, pp. 30-42, Nov.-Dec. 2018.
- [3] H. Cho et al., "A 79 pJ/b 80 Mb/s Full-Duplex Transceiver and a 42.5 μW 100 kb/s Super-Regenerative Transceiver for Body Channel Communication," in *IEEE Journal of Solid-State Circuits*, vol. 51, no. 1, pp. 310-317, Jan. 2016.
- [4] W. Saadeh, M. A. B. Altaf, H. Alsuradi and J. Yoo, "A 1.1-mW Ground Effect-Resilient Body-Coupled Communication Transceiver With Pseudo OFDM for Head and Body Area Network," in *IEEE Journal of Solid-State Circuits*, vol. 52, no. 10, pp. 2690-2702, Oct. 2017.
- [5] S. Maity, B. Chatterjee, G. Chang and S. Sen, "BodyWire: A 6.3-pJ/b 30-Mb/s 30-dB SIR-Tolerant Broadband Interference-Robust Human Body Communication Transceiver Using Time Domain Interference Rejection," in *IEEE Journal of Solid-State Circuits*, vol. 54, no. 10, pp. 2892-2906, Oct. 2019.
- [6] J. Park, H. Garudadri and P. P. Mercier, "Channel Modeling of Miniaturized Battery-Powered Capacitive Human Body Communication Systems," in *IEEE Transactions on Biomedical Engineering*, vol. 64, no. 2, pp. 452-462, Feb. 2017.
- [7] J. Park and P. P. Mercier, "Magnetic human body communication," in 2015 37th Annual International Conference of the IEEE Engineering in Medicine and Biology Society (EMBC), 2015, pp. 1841-1844.
- [8] J. W. Park and B. Razavi, "Channel Selection at RF Using Miller Bandpass Filters," in *IEEE Journal of Solid-State Circuits*, vol. 49, no. 12, pp. 3063-3078, Dec. 2014.